

State-specific ion mobilities of Lr^+ ($Z = 103$) in helium

Harry Ramanantoanina*,^{1,2} Anastasia Borschevsky,³ Michael Block,^{1,2,4} Larry Viehland,⁵ and Mustapha Laatiaoui^{†1,2}

¹ *Department Chemie, Johannes Gutenberg-Universität, Fritz-Strassmann Weg 2, 55128 Mainz, Germany*

² *Helmholtz-Institut Mainz, Staudingerweg 18, 55128 Mainz, Germany*

³ *Van Swinderen Institute for Particle Physics and Gravity, University of Groningen, Nijenborgh 4, 9747 Groningen, The Netherlands*

⁴ *GSI Helmholtzzentrum für Schwerionenforschung, Planckstrasse 1, 64291 Darmstadt, Germany*

⁵ *Science Department, Chatham University, Pittsburgh, Pennsylvania 15232, USA*

(Dated: July 7, 2023)

Ion mobilities of Lr^+ ($Z = 103$) and of its lighter chemical homolog Lu^+ ($Z = 71$) in helium were calculated for the ground state $^1\text{S}_0$ and the lowest metastable state $^3\text{D}_1$. To this end we applied the multi-reference configuration interaction (MRCI) method to calculate the ion-atom interaction potentials in the different states. The Gram-Charlier approach to solving the Boltzmann equation was used to deduce the mobilities of the different electronic states, based on the calculated interaction potentials. We found that the zero-field ion mobilities are similar for the Lr^+ and Lu^+ ions. In addition, the ion mobilities of the different states are substantially different for temperatures above 100 K. The relative differences between the mobilities of the ground and excited states at room temperature are about 15% and 13% for Lu^+ and Lr^+ ions, respectively, which should be sufficiently large enough to enable laser resonance chromatography (LRC) of these ions.

Keywords: Heavy and Superheavy Elements, Electronic structures, Relativistic Calculation, ion mobility

I. INTRODUCTION

Lawrencium is a synthetic element that was first discovered in 1961 by A. Ghiorso and colleagues and has since been placed 103rd in the periodic table as the heaviest actinide [1]. Interest in this element has not waned since then, motivated initially by new insights into the nuclear structure of its isotopes [2], and not least by the question of whether lawrencium, together with lutetium, are homologues of scandium and yttrium [3, 4]. Recently, it has gained special attention because its ionization potential has been studied for the first time [5] and laser spectroscopy has already reached its neighboring element nobelium [6, 7], element 102, which in turn raises hopes to also experimentally study the atomic structure of lawrencium [8]. The dramatic increase of relativistic effects with atomic number makes the ground state of this element adopt the $7s^27p_{1/2}$ ($^2\text{P}^{\circ}_{1/2}$) electron configuration, in contrast to lutetium, where the valence electron occupies the d orbital. Various theoretical predictions agree with high confidence on this ground-state configuration in Lr [2, 9–13], while experimental confirmation is still awaited.

In preparation for experiments, much theoretical work has been done in recent years to elucidate the atomic structure and ionization potential of neutral Lr [9–12], taking into account relativistic effects (including, in many

cases, the quantum electrodynamics corrections) and adequately addressing electron correlation. With the recent proposal to perform spectroscopy on superheavy ions using Laser Resonance Chromatography (LRC) techniques [14], the electronic structure of the singly charged ion has also come increasingly into focus [15–17].

In the LRC technique, the ions are subjected to pulsed laser beams for resonant optical pumping into metastable states before their release into a drift tube filled with helium gas. When the ions in different electronic states experience different interactions with helium atoms they move under the influence of an external and homogeneous electric field with different velocities through the drift tube toward the particle detector, enabling state-specific ion separation and resonance detection [14]. The transport properties of several actinide ions in noble gases have been studied already in Ref. [18], demonstrating the dependence of the ion mobility on the electronic configuration. In order to take advantage of the novel LRC approach, experimental conditions must be found such that the mobility of the ground state is substantially different from that of the excited state, which requires rigorous theoretical parameter confinement in advance [19]. So far, only the ground-state transport properties have been predicted for the Lr^+ ion, and the excited-state mobilities remain to be explored for optimal design of the experiment.

In previous work [20, 21], the multi-reference configuration interaction (MRCI) method provided reliable predictions of the energy levels for the ground and low-lying excited states of heavy metal ions, achieving theoretical uncertainties between 5 and 10%. In the current study

*Corresponding author: harry.ramanantoanina@kit.edu

†Corresponding author: mlaatiao@uni-mainz.de

we use the MRCI method to treat interatomic interactions; based on the obtained interaction potentials, we calculate the state-specific mobility of Lu^+ and Lr^+ ions drifting in helium gas in their ground (1S_0) and lowest excited (metastable 3D_1) electronic states.

II. METHODOLOGY AND COMPUTATIONAL DETAILS

The *ab initio* MRCI calculations of the interaction potentials ($V(d)$) were performed using the DIRAC19 code [22]. The calculations were carried out in the framework of the four component Dirac-Coulomb Hamiltonian, and the nuclei were treated within a finite-nucleus model *via* the Gaussian charge distribution [23]. The uncontracted Gaussian-type Dyall basis sets [24, 25] of single-augmented triple-zeta (s-aug-cv3z) quality were used for all the elements. The metal ion and the neutral helium atom were placed along the z -axis in a system of Cartesian coordinates, separated by an inter-atomic distance d that was varied from 2.0 Å to 40.0 Å for the calculation of the interaction potentials. We use the Boys-Bernardi counterpoise correction to tackle basis set superposition error [26]: $V(d) = E_{M^+-\text{He}}(d) - E_{M^+}(d) - E_{\text{He}}(d)$, with $M = \text{Lu}$ and Lr . $E_{M^+-\text{He}}(d)$ is the MRCI energy of the $M^+-\text{He}$ system at an inter-atomic distance d . $E_{M^+}(d)$ and $E_{\text{He}}(d)$ are the energies of the systems $M^+-\text{Gh}$ and $\text{Gh}-\text{He}$, respectively, where He and M atoms are replaced by a ghost atom (Gh) without charge but carrying the the full basis sets of the He and M elements, respectively.

The electronic structure was obtained in two steps. In the first step, Dirac-Hartree-Fock calculations were performed using the average of configuration (AOC) type calculation. The AOC allowed us to represent the open-shell electronic structure system with 2 valence electrons that were evenly distributed over 12 valence spinors (6 Kramers pairs) of s and d atomic characters. The resulting wavefunction was used as reference for the CI calculations. In the second step, the energy levels and the spectroscopic properties were calculated using the MRCI approach, within the Kramers-restricted configuration interaction (KRCI) module in DIRAC19 [22, 27–29]. In this implementation, the KRCI calculations use the concept of generalized active space (GAS) [30], which enables MRCI calculations with single and double electron excitations for different GAS set-ups [27]. The MRCI model *a priori* takes into consideration the dynamical correlation of the active electrons [31].

We report in Table I the GAS set-up together with the technical specifications that were important in the MRCI calculation. In total, we considered 4 GAS that were selectively chosen to activate 26 electrons within 21 semi-core and valence orbitals as well as virtual orbitals with energies below 30 atomic units, i.e. 194 and 199 for the Lu^+-He and Lr^+-He systems, respectively. Be-

TABLE I: Specification of the generalized active space (GAS) scheme used in the calculations of the Lu^+-He and Lr^+-He systems. See text for details.

GAS Space	Accumulated Electrons		Number of Kramers pairs	Characters ^a
	Min ^b	Max		
1	8- m	8	4	($n-1$) s , ($n-1$) p
2	24- q	24	8	($n-2$) f , He 1 s
3	24	26	9	ns , ($n-1$) d , np
4	26	26	≤ 30 a.u.	Virtual

^aFor Lu^+-He and Lr^+-He , $n = 6$ and 7 , respectively

^b m and q are variables that control the electron excitation process attributed to the selective GAS

cause the total number of configuration state functions was too large, we defined the parameters m and q to control the electron excitation process that occurred at the semi-core level. These parameters were set to $m=2$ and $q=1$, which signified that double- and single-electron excitations were allowed from the selective GAS. It is noteworthy to point out that truncated configuration interaction method is not size-consistent [32]. We did not explicitly use the Davidson (+Q) corrections [22] to solve this problem. But we surmise that including higher order excitation in the GAS scheme (see Table I) has helped to mitigate the size-consistency issue in the present MRCI method. Furthermore, we also employed size-extensive Fock space coupled cluster (FSCC) [22] to validate the MRCI method (*vide infra*).

To validate the MRCI results, we have also conducted calculations on the relativistic multireference FSCC level of theory. The relativistic FSCC approach is considered to be a very powerful method for the treatment of heavy atomic and small molecular systems and it is also available in DIRAC19 [22]; this method is particularly well-suited for treating systems with two valence electrons, via the sector(0,2) algorithm [33], such as Lu^+-He and Lr^+-He investigated here.

The FSCC calculation started with the closed-shell reference electronic state, that was, in our case, the $\text{Lr}^{3+}-\text{He}$ and $\text{Lu}^{3+}-\text{He}$ systems. For the sake of comparison, the FSCC computational details (relativistic method, basis sets, treatment of the nuclei) were the same as those used in the MRCI calculations (see above). In total, 60 and 74 core and semi-core electrons of the Lu^+ and Lr^+ ions, respectively, plus 2 He 1 s electrons, were correlated. Virtual orbitals up to energies of 30 atomic units were also included in the correlation space. Then, two electrons were added to the selected virtual orbitals (the model space) to obtain the singly ionized Lr^+-He and Lu^+-He systems, for which the appropriate coupled cluster equations were solved in an iterative way. Convergence difficulties were lifted by complementing the FSCC method with the intermediate Hamiltonian approach [33].

We described the electronic states that corresponded to the interaction potential between the heavy metal ions and the neutral He atom by means of the quantum numbers J and Ω , representing the total angular momentum of the metal ions and its projection onto the inter-atomic axis, respectively. In particular, we labelled the electronic states using the Hund's case (c) notation, i.e. Ω_J^σ , for consistency with conventional practice for the calculations of ion mobility and transport properties ($\sigma = +$ or $-$ is an additional notation proper to the linear $C_{\infty v}$ point group that represents the invariability of the wavefunction with respect to the σ_v symmetry operator) [18, 19]. Thus, the ground state 1S_0 of the free Lr^+ and Lu^+ ions give rise to the $\Omega = 0$ state in the $\text{Lr}^+\text{-He}$ and $\text{Lu}^+\text{-He}$ systems, i.e. $X0^+$. The metastable 3D_1 state, on the other hand, transformed to the non-degenerate 0_1^- and double-degenerate 1_1 states, since $\Omega = 0$ and ± 1 , respectively. Using the same notation, the next excited states 3D_2 and 3D_3 transformed to the single-degenerate 0_2^+ and 0_3^- as well as the double-degenerate 1_2 , 1_3 , 2_2 , 2_3 , and 3_3 states.

The ion mobilities were calculated from the ion-atom interaction potentials by solving the Boltzmann equation by the Gram-Charlier approach [34]. To this end we used the program PC [35], which delivers the momentum transfer and other transport cross sections as a function of the collision energy. From this we then calculated the reduced ion mobility K_0 either as a function of temperature at a given electric field-to-gas-number density (E/n_0) or as a function of E/n_0 at different temperatures, utilizing the program VARY [36]. Here K_0 is the ion mobility K normalized to the standard pressure P_0 and the standard temperature T_0 according to $K_0 = K \frac{P}{P_0} \frac{T_0}{T}$. Beyond $d = 40 \text{ \AA}$, the interaction potentials were adjusted to asymptotically mimic the long-range induced ion-dipole attraction given by $V_{pol}(d) = e^2 \alpha_p / (2(4\pi\epsilon_0)^2 d^4)$, with the static average dipole polarizability of helium of $\alpha_p = 0.205 \text{ \AA}^3$ [37].

For the 1S_0 ground state, there is only one potential per ionic species and thus a single mobility curve was obtained for each ion. For the 3D_1 excited state an isotropic averaged potential was first used to calculate the isotropic ion mobility K_0^{iso} , which we then compared with the averaged mobility K_0^{av} [18]. This latter was obtained by averaging the mobilities from interaction potentials for each Ω component with their statistical weights according to

$$K_0^{av}(T) = [K_0^{0_1^-}(T) + 2K_0^{1_1}(T)]/3. \quad (1)$$

In the Supplementary Material, Figure S1 shows the calculated isotropic ion mobilities together with the averaged ion mobilities corresponding to the 3D_1 state for both $\text{Lu}^+\text{-He}$ and $\text{Lr}^+\text{-He}$ systems.

III. RESULTS AND DISCUSSION

Table II lists the calculated energies of the ground (1S) and the metastable (3D) electronic states of the Lu^+ and Lr^+ obtained from the MRCI and the FSCC calculations. To calculate these energies following the models described in the Methodology section, we set the distance between the metal ion and the neutral atom to 40.0 \AA , which is large enough to make sure that the energy difference between the multiple components of the free ion multiplets are negligible, so that they are comparable to atomic energies. For Lu^+ , experimental data are also listed for comparison. The two theoretical models at hand yield similar results, with good agreement with the experiments and previous theoretical data [16, 21]. The good agreement with both the experimental values and the FSCC results confirms the suitability of MRCI for electronic structure calculations of heavy metal ions.

TABLE II: Calculated low-lying energy levels of $\text{Lu}^+\text{-He}$ and $\text{Lr}^+\text{-He}$ ions (in cm^{-1}) obtained from the FSCC and MRCI calculations (the separation distance between the metal Lu^+/Lr^+ ions and He are set to 40.0 \AA , showing the energy of the ground state 1S and metastable states 3D of the metal ions.). For $\text{Lu}^+\text{-He}$, the experimental energy values reported for the Lu^+ ion is also listed for comparison.

$^{2S+1}L_J$	Ω_J^σ	Lu^+			Lr^+	
		FSCC	MRCI	Exp. ^a	FSCC	MRCI
1S_0	$X0^+$	0	0	0	0	0
3D_1	$0_1^- + 1_1$	12354	12184	11796	20265	21751
3D_2	$0_2^+ + 1_2 + 2_2$	12985	12642	12435	21623	22442
3D_3	$0_3^- + 1_3 + 2_3 + 3_3$	14702	13881	14199	26210	24708

^ataken from ref. [38]

The calculated interaction potentials of the ground and the metastable electronic states of $\text{Lu}^+\text{-He}$ and $\text{Lr}^+\text{-He}$ are shown in Figure 1. Since the MRCI and FSCC calculations are both based on the relativistic Dirac-Coulomb Hamiltonian and employ the same basis sets, the discrepancies between the two sets of calculations can be interpreted in terms of the treatment of electron correlation. There is a good agreement between the FSCC and MRCI data of the ground-state $X0^+$ (1S_0) for both $\text{Lr}^+\text{-He}$ and $\text{Lu}^+\text{-He}$ systems. For the latter, the ground-state interaction potentials are also comparable with the scalar-relativistic potentials reported in Refs.[18, 19]. However, we obtain larger discrepancies between the two methods for the metastable states, namely in the 1_1 (3D_1).

The *ab initio* interaction potentials are fitted by the Morse potential energy function [39],

$$V(d) = D_e(e^{-2\alpha(d-d_{min})} - 2e^{-\alpha(d-d_{min})}) \quad (2)$$

to derive the the equilibrium inter-atomic distance (d_{min}), the dissociation energy (D_e), and the range

parameter α . These are listed in Table III and Table IV. The energy splitting between the 1_1 and 0_1^- (3D_1) metastable states in the short-range interaction is larger in the FSCC data. Thus we see a slight shift of the equilibrium distances (d_{min}) to smaller values from the MRCI to the FSCC 1_1 (3D_1) interaction potentials: 0.06 Å and 0.12 Å for the Lu^+ -He and Lr^+ -He systems, respectively. We also see a slightly higher FSCC dissociation energy of this state in Lr^+ -He.

The calculated d_{min} values by the two models follow the same trend in the Lu^+ -He (Table III) and Lr^+ -He (Table IV) systems: d_{min} associated with the $X0^+$ (1S_0) ground state is larger compared with the two 1_1 and 0_1^- (3D_1) metastable states. We can compare the spectroscopic parameters for Lu^+ -He in both the ground and metastable states (cf. Table III) as well as Lr^+ -He in the ground state (cf. Table IV) to earlier coupled cluster studies [18, 19]. We find that the present d_{min} values (both MRCI and the FSCC values) are slightly larger (+2.5%) than the results reported in the aforementioned Refs. [18, 19] for the ground and the metastable states.

The dissociation energy (D_e) calculated within the MRCI and the FSCC models also follows a similar trend in the two systems. The metastable 0_1^- (3D_1) shows the weakest interaction, whereas its counterpart 1_1 (3D_1) state has the strongest. This is in contrast to the earlier predictions (Table III), where the calculated D_e for the 0_1^- and 1_1 (3D_1) metastable states in Lu^+ -He are very close (with an energy difference of 2.3 cm^{-1} only). This energy difference is 6.94 cm^{-1} and 13.1 cm^{-1} , respectively, for the present MRCI and FSCC results (Table III). This disagreement with previous calculations could be due to the difference in the treatment of relativistic effects. We used the four-component DCHF-based model as a basis of our calculations, whereas in Ref. [19], the spin-orbit coupling is treated within perturbation theory based on a scalar relativistic electronic structure. However, the many different computational parameters (choice of basis set and the correlation space and the treatment of correlation) make direct comparison between these values difficult. Overall, the bonding interaction between the metal ion and the helium atom is shown to be very weak, regardless of the theoretical approach.

The ion mobilities were calculated based on the interaction potentials obtained from the MRCI calculations. Figure 2 shows an overview of the obtained zero-field mobilities of Lu^+ and Lr^+ in helium as function of the gas temperature. We have also calculated the ion mobilities based on the FSCC interaction potentials. In the Supplementary Material (Figure S2), a comparison between mobilities obtained with the MRCI and FSCC interaction potentials are also presented. In general, the mobilities of the ground states of the two ions obtained based on the different *ab initio* approaches agree well with each other. In addition a good agreement of the Lu^+ -He and Lr^+ -He

TABLE III: Calculated spectroscopic dissociation energy D_e (in cm^{-1}), equilibrium distance d_{min} (in Å), and range parameters α (in $1/\text{Å}$) of the interaction potential of Lu^+ -He corresponding to the Lu^+ 1S_0 and 3D_1 electronic states obtained by a mathematical fit to Equation 2, and compared with previous calculations (Ref.).

Lu^+ -He		MRCI			FSCC			Ref. ^a	
		D_e	d_{min}	α	D_e	d_{min}	α	D_e	d_{min}
1S_0	$X0^+$	45.23	4.224	1.213	42.71	4.264	1.197	47.3	4.17
3D_1	0_1^-	42.13	4.171	1.133	39.16	4.187	1.123	49.9	4.11
	1_1	49.07	4.006	1.114	52.26	3.948	1.075	52.2	3.91

^ataken from ref. [19]

TABLE IV: Calculated spectroscopic dissociation energy D_e (in cm^{-1}), equilibrium distance d_{min} (in Å), and range parameters α (in $1/\text{Å}$) of the interaction potential of Lr^+ -He corresponding to the Lr^+ 1S_0 and 3D_1 electronic states, obtained by a mathematical fit to Equation 2, and compared with previous calculations (Ref.).

Lr^+ -He		MRCI			FSCC			Ref. ^a	
		D_e	d_{min}	α	D_e	d_{min}	α	D_e	d_{min}
1S_0	$X0^+$	46.78	4.134	1.192	48.59	4.179	1.205	52	4.08
3D_1	0_1^-	39.49	4.177	1.118	43.92	4.108	1.174		
	1_1	51.84	3.880	1.094	72.37	3.756	1.111		

^ataken from ref. [18]

ground-state mobilities is achieved with those reported in Refs. [18, 19]

The principal difference between the two method concerns the $\Omega = 1$ components; the MRCI calculations result in smaller dissociation energies at larger equilibrium distances (see Table III and Table IV) and thus in smaller state-specific reduced mobilities compared with the FSCC based predictions, see also the Supplementary Material Figure S2. For brevity we discuss here only the mobility results obtained from predictions based on the MRCI interaction potentials; the minor differences between the MRCI and FSCC results mean that the conclusions of this work are not dependent on the computational approach.

The mobilities of the two systems are distinct for the different ionic states in a wide temperature range and converge towards the polarization limit $K_{pol} = (13.876/\alpha_p^{1/2})[(M_{He} + M_{ion})/M_{He}M_{ion}]^{1/2}$ at about 15.5 cm^2/Vs in the mK temperature regime [41]. Here, the number 13.876 is obtained when α_p is given in units of Å^3 and the masses M are in atomic mass units. The mobility increases with increasing temperature to reach a local maximum at 100 K for the ions in the 1S_0 ground state ($X0^+$) before it decreases below 13 cm^2/Vs at temperatures beyond 1000 K. The predicted mobility for Lu^+ in the ground state is found to be in excellent agreement with the only available experimental data reported for a

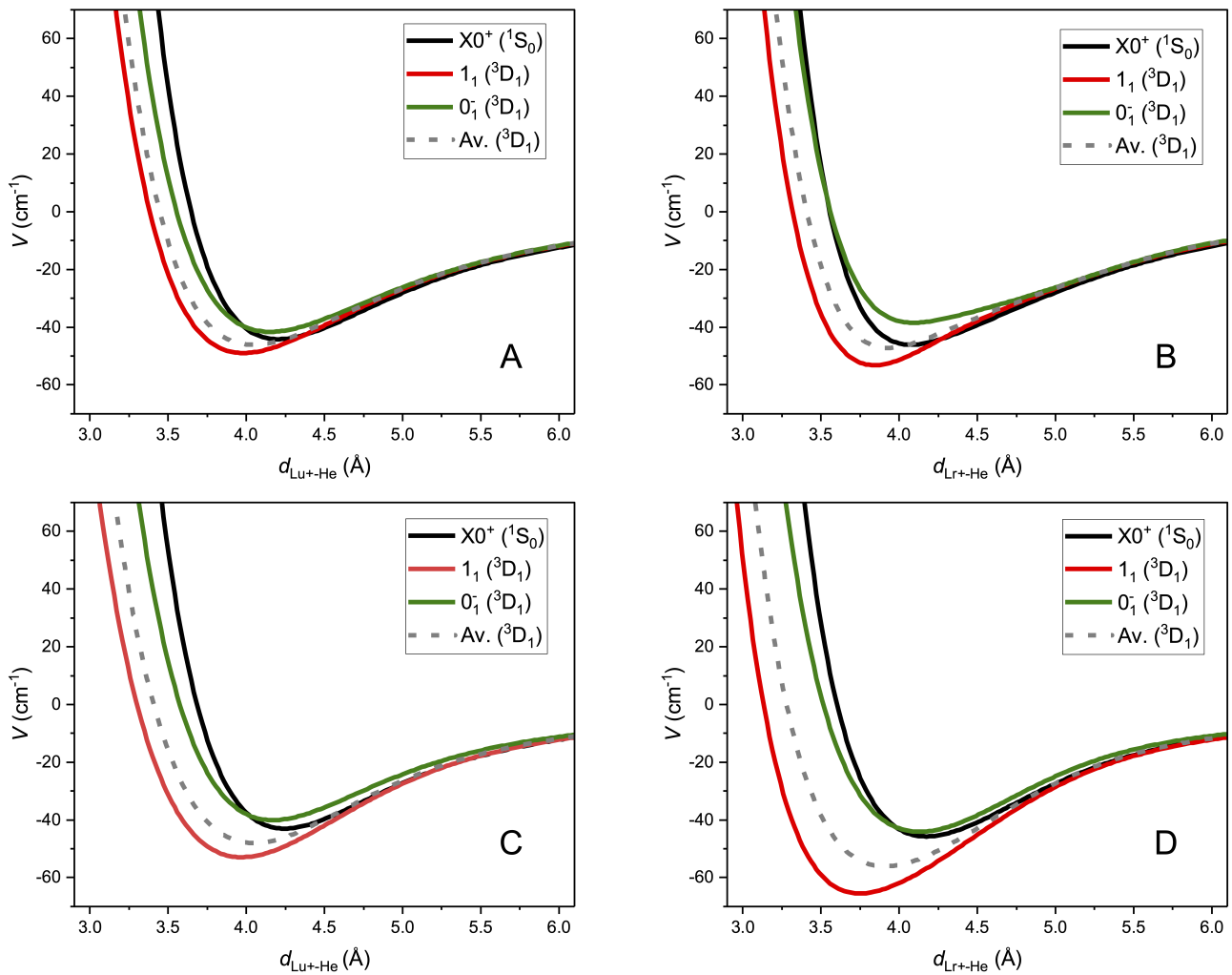


FIG. 1: Graphical representations of the MRCI interaction potentials of the $\text{Lu}^+\text{-He}$ (A) and $\text{Lr}^+\text{-He}$ (B) systems, compared with the FSCC interaction potentials of $\text{Lu}^+\text{-He}$ (C) and $\text{Lr}^+\text{-He}$ (D). In each panel, the ground XO^+ (1S_0) (solid black curve), and the two low-lying metastable 1_1 (3D_1) (red) 0_1 (3D_1) (green) states are represented, together with the calculated average interaction potential for the metastable states (dashed grey curve). Note that for clarity the potentials are normalized to the same dissociation limit.

temperature of 295 K [40].

For the ions in the 3D_1 states we calculated the mobilities for each of the Ω components, 0_1^- and 1_1 , to deduce the average mobility K_0^{av} according to Equation 1. The resulting curves are indicated with dashed lines in Figure 2. Although these average mobilities are deemed to be more accurate than the isotropic ones [18] we found that both mobilities are in excellent agreement with each other for the two ion species, Lu^+ and Lr^+ in the 3D_1 states, see the Supplementary Material Figure S1. Similarly to the ground state mobilities, the average excited state mobility increases with increasing temperature to reach a maximum at about 105 K for both ions before it decreases towards higher temperatures. Noteworthy, however, is the difference in zero-field mobility between the ground state and the average mobility of the excited state: e.g., 14.8% and 13% at room temperature for the

$\text{Lu}^+\text{-He}$ and $\text{Lr}^+\text{-He}$ systems, respectively, with a tendency of increasing relative differences towards higher temperatures.

In Figure 3 we show the reduced mobilities of the different states of Lu^+ and Lr^+ obtained based on the MRCI interaction potentials for different gas temperatures as a function of the electric-field-to-gas-number density E/n_0 (the so-called reduced electric field, which is given in units of Townsend, $1 \text{ Td} = 10^{-17} \text{ V cm}^2$). In the Supplementary Material, Figure S3 shows a comparison between the ion mobilities calculated with the MRCI and FSCC interaction potentials. In general, the mobility is roughly constant at reduced fields below 10 Td, such that it depends mainly on the gas temperature, with a tendency of being larger at lower temperatures (down to 100 K). As the reduced field increases, the ion mobility decreases almost exponentially to values below $12 \text{ cm}^2/\text{Vs}$

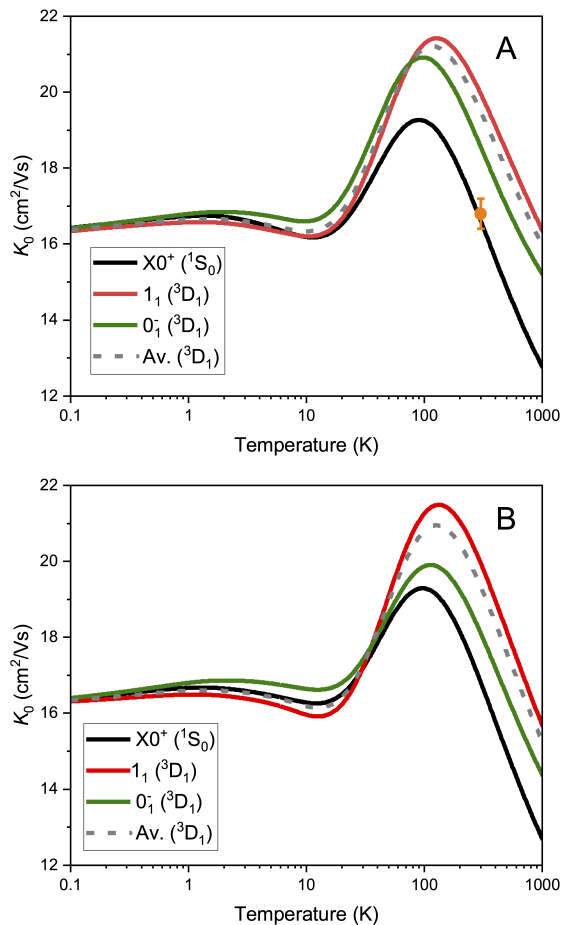


FIG. 2: Reduced zero-field mobilities of the $\text{Lu}^+\text{-He}$ (A) and $\text{Lr}^+\text{-He}$ (B) systems in the ground $X0^+$ (1S_0) (in black), as well as in the metastable 1_1 (3D_1) (in red) and the 0_1^- (3D_1) (in green) states as a function of the temperature, derived from the MRCI interaction potential. The calculated average mobilities for the metastable states (3D_1) are also depicted (in grey); the data point that represents the experimental result for the ground state of Lu^+ ion is also shown (orange dot and error bar) [40].

at $E/n_0 \geq 100$ Td for the ions in the ground states. It nearly decouples from the temperature dependency at extremely large E/n_0 values as the energy gained from the electric field dominates the effective ion temperature. The average mobility for the excited states exhibits a similar behavior as a function of the reduced field. Although the 0-orbital-projection components have rather small mobilities, close to those of the ground states, the average mobilities of the excited states are dominated by the $\Omega = 1$ component, due its higher multiplicity (Equation 1), see also the Supplementary Material Figure S4. Similar reduced mobilities were obtained for both investigated ionic species, Lu^+ and Lr^+ , in the 3D_1 state, as can be seen in Figure 3.

In order to reach significant time resolution in future LRC applications the relative drift time differences, due

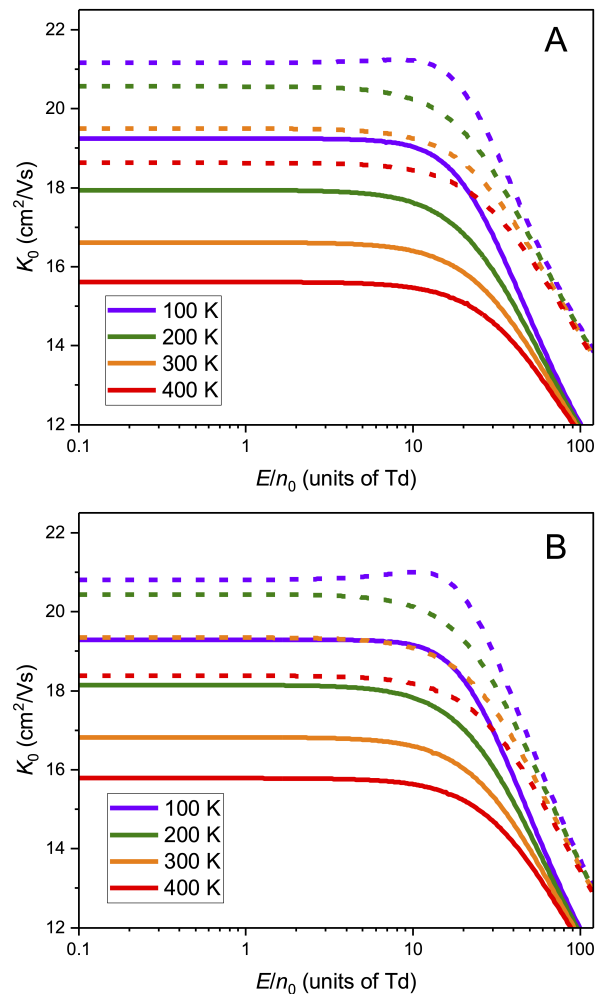


FIG. 3: Reduced mobilities of the $\text{Lu}^+\text{-He}$ (A) and $\text{Lr}^+\text{-He}$ (B) systems as function of E/n_0 and at selected temperatures, derived from the MRCI interaction potential, corresponding to the ground $X0^+$ (1S_0) (solid lines) and the metastable 3D_1 (dashed lines) states. For the metastable states, the depicted mobility curves correspond to the average calculated mobility of the 1_1 and the 0_1^- electronic states obtained using Equation 1 (See also the Supplementary Material, Figure S4).

to the relative mobility differences, have to be maximized [19]. Our results suggest a similar trend for both investigated ionic species, see Figure 4. At gas temperatures above 100 K the relative mobility differences for the ground and excited states are between 7% and 17% at reduced fields below 200 Td, with a tendency of becoming larger for higher temperatures. These differences stay above 12% at room temperature and become rather insensitive to the reduced E/n_0 field at 400 K.

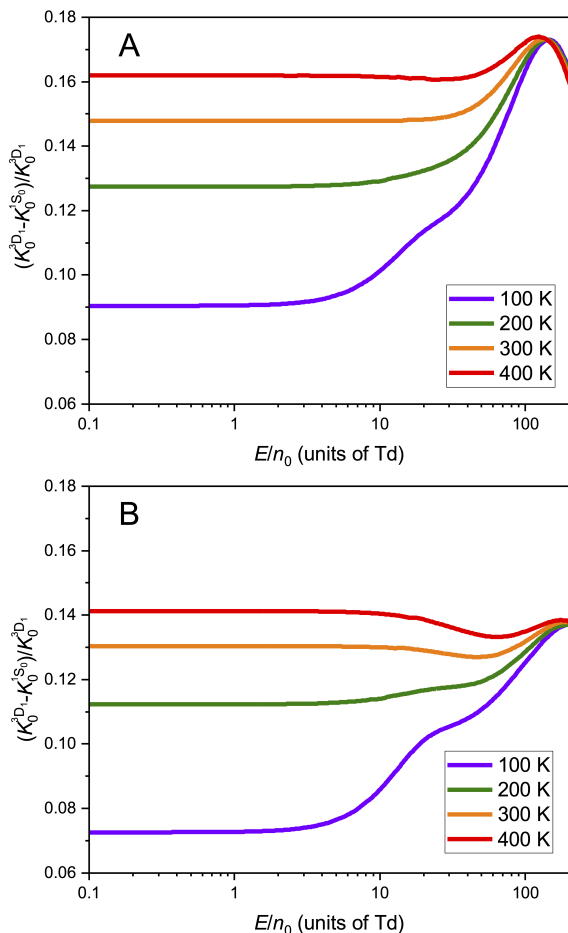


FIG. 4: Relative differences between the reduced mobilities of the ground and the average metastable states of the $\text{Lu}^+\text{-He}$ (A) and $\text{Lr}^+\text{-He}$ (B) systems as function of E/n_0 at selected temperatures, derived from the MRCI interaction potentials.

IV. SUMMARY AND CONCLUSION

We have carried out MRCI and FSCC calculations of the interaction potentials of the $\text{Lr}^+\text{-He}$ and $\text{Lu}^+\text{-He}$ systems. Based on these potentials we predicted the ion mobility of Lu^+ and Lr^+ ions in helium gas, and found the two approaches to be in excellent agreement, justify-

ing the use of either method in future investigations. In particular, the MRCI-based method for calculating interaction potentials and ion mobilities will be relevant for the study of the $\text{Rf}^+\text{-He}$ systems, which will be the next step of our theoretical work.

The predicted ion mobility value for Lu^+ in the ground state at room-temperature is in a striking agreement with the experimentally reported one [42]. Similar accuracy can be expected for the room temperature mobility of Lr^+ , at least in its ground state, due to the similarities of their electronic structures. As long as the reduced fields are below 200 Td, we expect the relative drift time differences to be above 7%; the higher the gas temperature the larger these differences become. Laser resonance chromatography on both ionic species should thus be feasible in terms of time resolution already at room temperature, i.e., without involving sophisticated cryogenic ion mobility spectrometers. Since quenching of states may become strong at elevated effective ion temperatures [19], one may prefer to apply moderate reduced fields below 40 Td and room temperature gas environments in order to maintain state populations in the envisaged LRC experiments [43]. In such a case we expect relative drift time differences between ground and metastable states to be about 15% and 13% for Lu^+ and Lr^+ , respectively, which should enable disentangling the different drift behaviours upon resonant excitations.

V. ACKNOWLEDGEMENTS

This project has received funding from the European Research Council (ERC) under the European Union’s Horizon 2020 Research and Innovation Programm (Grant Agreement No. 819957). We also gratefully acknowledge high performance computing (HPC) support, time and infrastructure provided by: SURFsara HPC at Snellius via the HPC-Europa3 programm, the Center for Information Technology of the University of Groningen (Peregrine), the Johannes Gutenberg University of Mainz (Mogon), and the HPC group of GSI. We thank Alexei Buchachenko for useful discussion.

-
- [1] A. Ghiorso, T. Sikkeland, A. Larsh, and R. Latimer, *Phys. Rev. Lett.* **6**, 473 (1961).
 - [2] M. Asai, F. P. Heßberger, and A. Lopez-Martens, *Nucl. Phys.* **A944**, 308 (2015).
 - [3] W. Jensen, *J. Chem. Educ.* **59**, 634 (1982).
 - [4] E. Scerri, *Journal of Chemical Education* **86**, 1188 (2009).
 - [5] T. Sato, M. Asai, A. Borschevsky, T. Stora, N. Sato, Y. Kaneya, K. Tsukada, C. E. Düllmann, K. Eberhardt, E. Eliav, et al., *Nature* **520**, 209 (2015).
 - [6] M. Laatiaoui, W. Lauth, H. Backe, M. Block, D. Ackermann, B. Cheal, P. Chhetri, C. E. Düllmann, P. Van Duppen, J. Even, et al., *Nature* **538**, 495 (2016).
 - [7] P. Chhetri, D. Ackermann, H. Backe, M. Block, B. Cheal, C. Droese, C. E. Düllmann, J. Even, R. Ferrer, F. Giacoppo, et al., *Physical Review Letters* **120** (2018).
 - [8] M. Laatiaoui and S. Raeder, *Nucl. Phys. News* **29**, 21 (2019).
 - [9] A. Borschevsky, E. Eliav, M. J. Vilkas, Y. Ishikawa, and U. Kaldor, *Eur. Phys. J. D* **45**, 115 (2007).

- [10] S. Fritzsche, C. Z. Dong, F. Koike, and A. Uvarov, *Eur. Phys. J. D* **45**, 107 (2007).
- [11] V. A. Dzuba, M. S. Safronova, and U. I. Safronova, *Phys. Rev. A* **90**, 012504 (2014).
- [12] E. V. Kahl, S. Raeder, E. Eliav, A. Borschevsky, and J. C. Berengut, *Phys. Rev. A* **104**, 052810 (2021), URL <https://link.aps.org/doi/10.1103/PhysRevA.104.052810>.
- [13] W.-H. Xu and P. Pyykkö, *Phys. Chem. Chem. Phys.* **18**, 17351 (2016), URL <http://dx.doi.org/10.1039/C6CP02706G>.
- [14] M. Laatiaoui, A. A. Buchachenko, and L. A. Viehland, *Phys. Rev. Lett.* **125**, 023002 (2020).
- [15] E. Paez, K. J. Arnold, E. Hajiyev, S. G. Porsev, V. A. Dzuba, U. I. Safronova, M. S. Safronova, and M. D. Barrett, *Phys. Rev. A* **93**, 042112 (2016).
- [16] E. V. Kahl, J. C. Berengut, M. Laatiaoui, E. Eliav, and A. Borschevsky, *Physical Review A* **100** (2019).
- [17] B. Lackenby, V. Dzuba, and V. Flambaum, *Phys. Rev. A* **101**, 012514 (2020).
- [18] G. Visentin, M. Laatiaoui, L. Viehland, and A. Buchachenko, *Frontier in Chemistry* **8**, 438 (2020).
- [19] M. Laatiaoui, A. Buchachenko, and L. A. Viehland, *Phys. Rev. A* **102**, 013106 (2020).
- [20] H. Ramanantoanina, A. Borschevsky, M. Block, and M. Laatiaoui, *Phys. Rev. A* **104**, 022813 (2021), URL <https://link.aps.org/doi/10.1103/PhysRevA.104.022813>.
- [21] H. Ramanantoanina, A. Borschevsky, M. Block, and M. Laatiaoui, *Atoms* **10** (2022), ISSN 2218-2004, URL <https://www.mdpi.com/2218-2004/10/2/48>.
- [22] DIRAC, a relativistic ab initio electronic structure program, Release DIRAC19 (2019), written by A. S. P. Gomes, T. Saue, L. Visscher, H. J. Aa. Jensen, and R. Bast, with contributions from I. A. Aucar, V. Bakken, K. G. Dyall, S. Dubillard, U. Ekström, E. Eliav, T. Enevoldsen, E. Faßhauer, T. Fleig, O. Fossgaard, L. Halbert, E. D. Hedegård, B. Heimlich–Paris, T. Helgaker, J. Henriksson, M. Iliaš, Ch. R. Jacob, S. Knecht, S. Komorovský, O. Kullie, J. K. Lærdahl, C. V. Larsen, Y. S. Lee, H. S. Nataraj, M. K. Nayak, P. Norman, G. Olejniczak, J. Olsen, J. M. H. Olsen, Y. C. Park, J. K. Pedersen, M. Pernpointner, R. di Remigio, K. Ruud, P. Salek, B. Schimmelpfennig, B. Senjean, A. Shee, J. Sikkema, A. J. Thorvaldsen, J. Thyssen, J. van Stralen, M. L. Vidal, S. Villaume, O. Visser, T. Winther, and S. Yamamoto (available at <http://dx.doi.org/10.5281/zenodo.3572669>, see also <http://www.diracprogram.org>).
- [23] L. Visscher and K. G. Dyall, *Atom. Data Nucl. Data Tabl.* **67**, 207 (1997), URL <http://link.aps.org/doi/10.1103/PhysRevA.60.4439>.
- [24] K. G. Dyall, *Theoretical Chemistry Accounts* **112**, 403 (2004), URL <https://doi.org/10.1007/s00214-004-0607-y>.
- [25] K. G. Dyall, *Theoretical Chemistry Accounts* **129**, 603 (2011), URL <https://doi.org/10.1007/s00214-011-0906-z>.
- [26] S. Boys and F. Bernardi, *Molecular Physics* **19**, 553 (1970), URL <https://doi.org/10.1080/00268977000101561>.
- [27] T. Saue, R. Bast, A. S. P. Gomes, H. J. A. Jensen, L. Visscher, I. A. Aucar, R. Di Remigio, K. G. Dyall, E. Eliav, E. Fasshauer, et al., *The Journal of Chemical Physics* **152**, 204104 (2020), <https://doi.org/10.1063/5.0004844>, URL <https://doi.org/10.1063/5.0004844>.
- [28] J. Thyssen, T. Fleig, and H. J. A. Jensen, *The Journal of Chemical Physics* **129**, 034109 (2008), <https://doi.org/10.1063/1.2943670>, URL <https://doi.org/10.1063/1.2943670>.
- [29] S. Knecht, H. J. A. Jensen, and T. Fleig, *The Journal of Chemical Physics* **132**, 014108 (2010), <https://doi.org/10.1063/1.3276157>, URL <https://doi.org/10.1063/1.3276157>.
- [30] T. Fleig, J. Olsen, and L. Visscher, *The Journal of Chemical Physics* **119**, 2963 (2003), <https://doi.org/10.1063/1.1590636>, URL <https://doi.org/10.1063/1.1590636>.
- [31] T. Fleig, *Chemical Physics* **395**, 2 (2012), ISSN 0301-0104, recent *Advances and Applications of Relativistic Quantum Chemistry*, URL <https://www.sciencedirect.com/science/article/pii/S0301010411002710>.
- [32] P. G. Szalay, T. Müller, G. Gidofalvi, H. Lischka, and R. Shepard, *Chemical Reviews* **112**, 108 (2012), pMID: 22204633, <https://doi.org/10.1021/cr200137a>, URL <https://doi.org/10.1021/cr200137a>.
- [33] A. Landau, E. Eliav, Y. Ishikawa, and U. Kaldor, *The Journal of Chemical Physics* **121**, 6634 (2004), <https://doi.org/10.1063/1.1788652>, URL <https://doi.org/10.1063/1.1788652>.
- [34] L. A. Viehland, *Gaseous Ion Mobility, Diffusion, and Reaction* (Springer, 2018).
- [35] L. A. Viehland and Y. Chang, *Comput. Phys. Commun.* **181**, 1687 (2010).
- [36] L. A. Viehland, *Int. J. Ion Mobility Spectrom.* **15**, 21 (2012).
- [37] R. C. Weast and D. R. Lide, *CRC Handbook of Chemistry and Physics* (CRC Press, 1989), 70th ed.
- [38] A. Kramida, Yu. Ralchenko, J. Reader, and NIST ASD Team, NIST Atomic Spectra Database (ver. 5.10), [Online]. Available: <https://physics.nist.gov/asd> [2023, April 10]. National Institute of Standards and Technology, Gaithersburg, MD. (2022).
- [39] P. M. Morse, *Phys. Rev.* **34**, 57 (1929), URL <https://link.aps.org/doi/10.1103/PhysRev.34.57>.
- [40] M. J. Manard and P. R. Kemper, *International Journal of Mass Spectrometry* **412**, 14 (2017).
- [41] L. Viehland, E. Mason, W. Morrison, and M. Flannery, *Atomic Data and Nuclear Data Tables* **16**, 495 (1975).
- [42] M. J. Manard and P. R. Kemper, *International Journal of Mass Spectrometry* **423**, 54 (2017).
- [43] E. Romero-Romero, M. Block, B. Jana, E. Kim, S. Nothhelfer, S. Raeder, H. Ramanantoanina, E. Rickert, J. Schneider, P. Sikora, et al., *Atoms* **10**, 87 (2022).